Journal of Molecular Liquids 211 (2015) 1000–1008

Contents lists available at ScienceDirect

Journal of Molecular Liquids

journal homepage: www.elsevier.com/locate/molliq

Corrosion inhibition of carbon steel in aggressive acidic media with 1-(2-(4-chlorophenyl)-2-oxoethyl)pyridazinium bromide

Abderrahman Bousskri [a], Ali Anejjar [a], Mouslim Messali [b], Rachid Salghi [a,*], Omar Benali [c], Yasser Karzazi [d], Shehdeh Jodeh [e,*], Mohamed Zougagh [f], Eno.E. Ebenso [g], Belkheir Hammouti [d]

[a] Laboratory of Environmental Engineering and Biotechnology, ENSA, University Ibn Zohr, Box 1136, 80000 Agadir, Morocco
[b] Chemistry Department, Faculty of Science, Taibah University, 30002 Al-Madinah, Al-Mounawwara, Saudi Arabia
[c] Département de Biologie, Faculté des sciences et de la technologie, Université Dr. Tahar Moulay, Saïda, Algeria
[d] Laboratory of Applied Chemistry and Environment (URAC 18), Faculty of Sciences, University Mohammed Premier, B.P. 4808, 60046 Oujda, Morocco
[e] Department of Chemistry, An-Najah National University, P.O. Box 7, Nablus, Palestine
[f] Regional Institute for Applied Chemistry Research, IRICA, Av. Camilo Jose'Cela 10, E-13004 Ciudad Real, Spain
[g] Material Science Innovation & Modelling (MaSIM) Research Focus Area, Faculty of Agriculture, Science and Technology, North-West University (Mafikeng Campus), Private Bag X2046, Mmabatho 2735, South Africa

ARTICLE INFO

Article history:
Received 26 June 2015
Accepted 13 August 2015
Available online 27 August 2015

Keywords:
Acid medium
Adsorption
Pyridazinium-based ionic liquid
Carbon steel
Corrosion inhibition

ABSTRACT

Corrosion inhibition of carbon steel in 1.0 M HCl was investigated in the absence and the presence of different concentrations of 1-(2-(4-chlorophenyl)-2-oxoethyl)pyridazinium bromide (CPEPB). This inhibitive action against the corrosion of carbon steel in 1.0 M HCl solution was investigated at 298 K using gravimetric and electrochemical measurements. The effect of temperature on the corrosion behavior with the addition of CPEPB in the range of temperature from 298 to 328 K. The inhibition efficiency decreases slightly with the increase in the temperature. Results show that CPEPB is a good inhibitor and inhibition efficiency reach 91% at 10^{-3} M. The adsorption of this compound on carbon steel surface obeys Langmuir's adsorption isotherm. The kinetic and thermodynamic parameters were determined and discussed. Quantum chemical approach, using the density functional theory (DFT), was implemented in order to get a better understanding about the relationship between the inhibition efficiency and molecular structure of CPEPB and the calculated quantum chemical parameters were discussed.

1. Introduction

Protection against corrosion, the electrochemical destruction of metallic structures occurring through gradual anodic dissolution, represents a vital concern for many industries. This phenomena is typically favored on less noble metals (mainly iron, aluminum, copper, zinc, magnesium and their alloys) when exposed to corrosive environment such as acids. Hydrochloric acid (HCl) is widely used in removing scale and salts from steel surfaces, cleaning tanks and pipelines and steel alloys [1]. Because of the general aggression of acid solutions, inhibitors are commonly used to delay the corrosive attack on metallic materials. Over the years, tremendous efforts have been deployed aiming at finding suitable organic and inorganic corrosion inhibitors in various corrosive media [2–8]. The most effective are organic compounds containing electronegative functional groups and π-electron in triple or conjugated double bonds as well as heteroatom like phosphorus, sulphur, oxygen and nitrogen are major active adsorption centers [9–12]. The adsorption mode depends on the chemical composition of the solution, the chemical structure of the molecule; the electrochemical potential of the metal-solution interface and the nature of the metal surface. The most important aspect of inhibition, normally considered by corrosion scientists is the relation between corrosion inhibition efficiency and the molecular structure [13–15]. Ionic liquid (IL) compounds are emerging solvents like smart and excellent one, which are made of positive and negative ions that pack so badly together that they become liquids close to the room temperature [16–18]. They offer important properties such as high thermal stability, negligible vapor pressure, lack of inflammability, non-coordinating but good solvating ability, decent solubility for organic and inorganic compounds, a wide electrochemical potential window and high ionic conductivity [19–25]. Apart from these features each IL shows unique chemical and physical property by properly varying its cation and anion [26]. Therefore, they are considered as environmentally friendly alternatives to the classical use of organic solvents [27]. It has been reported that some ILs based on imidazolium, pyridinium and pyridazinium exhibited corrosion inhibition properties for the corrosion of various metals [28–38]. The present work aims at investigating the corrosion inhibition of carbon steel in 1.0 M HCl solution by 1-(2-(4-chlorophenyl)-2-oxoethyl)pyridazinium bromide (CPEPB) (Fig. 1)

* Corresponding author.
E-mail addresses: r.salghi@uiz.ac.ma (R. Salghi), sjodeh@hotmail.com (S. Jodeh).

http://dx.doi.org/10.1016/j.molliq.2015.08.038
0167-7322/

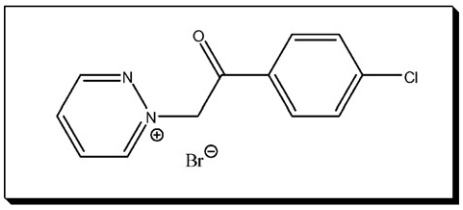

Fig. 1. Structural compound of inhibitor 1-(2-(4-chlorophenyl)-2-oxoethyl)pyridazinium bromide (CPEPB).

2. Materials and methods

2.1. Materials

The metal used in this study is a carbon steel (C38) (Euronorm: C35E carbon steel and US specification: SAE 1035) with a chemical composition (in wt.%) of 0.370% C, 0.230% Si, 0.680% Mn, 0.016% S, 0.077% Cr, 0.011% Ti, 0.059% Ni, 0.009% Co, 0.160% Cu and the remainder iron (Fe).

2.2. Synthesis of 1-(2-(4-chlorophenyl)-2-oxoethyl)pyridazinium bromide (CPEPB) under Ultrasonic irradiation

Though 1-(2-(4-chlorophenyl)-2-oxoethyl) pyridazinium bromide have been previously reported by conventional methods [39], its preparation under ultrasound irradiation was never revealed. Pyridazine (1 eq) and 2-bromo-1-(4-chlorophenyl)ethanone (1 eq) were placed in a closed container and exposed to irradiation for 5 h at 70 °C using a sonication bath. Completion of the reaction was performed by the precipitation of a solid from the initially obtained clear and homogenous mixture in toluene. The product is isolated by filtration and washed three times with ethyl acetate to remove any unreacted starting materials and solvent. Subsequently, the imidazolium salt was washed with ethyl acetate. Finally the IL compound was dried at a reduced pressure to remove all volatile organic compounds.

1-(2-(4-chlorophenyl)-2-oxoethyl)pyridazinium bromide (CPEPB) was characterized by ^{13}C NMR^{1}H NMR, IR and LCMS. ^{13}C NMR (100 MHz) and ^{1}H NMR (400 MHz) spectra were measured in DMSO at room temperature. Chemical shifts (δ) were reported in ppm calibrated to tetramethylsilane (TMS) as an internal standard. IR spectra were recorded in NaCl disc on a Shimadzu 8201 PC FTIR spectrophotometer (ν_{max} in cm^{-1}). LCMS spectra were measured with a Micromass LCT mass spectrometer. The ultrasound-assisted reactions were performed using a high intensity ultrasonic processor SUB Aqua 5 Plus-Grant with temperature controller (750 W), microprocessor control, and 25 kHz ultrasonic frequency.

2.3. Characterization of 1-(2-(4-chlorophenyl)-2-oxoethyl)pyridazinium bromide (CPEPB)

Brown crystals, yield 80%, ^{1}H NMR (400 MHz, CDCl3) δ: 6.87 (s, 2H), 7.75 (dd, 2H), 8.13 (dd, 2H), 8.82 (dd, 1H), 8.94 (dd, 1H), 9.78 (dd, 1H), 10.05 (dd, 1H) (Fig. 2); ^{13}C NMR (100 MHz, CDCl3) δ: 189.5 (CO), 154.6 (CH), 151.8 (CH), 139.7 (C), 137.5 (CH), 135.9 (CH), 132.0 (C), 130.3 (CH), 129.2 (CH), 70.2 (CH_2) (Fig. 3); IR(ν_{max} cm^{-1}) 3130 (C–H, sp 2), 1638 (C═O), 1598–1470 (C═C), 1166(C–N); LCMS (M–Br) 233.51 found for $C_{12}H_{10}ClN_2O^+$.

2.4. Weight loss measurements

The carbon steel specimens of $2 \times 2 \times 0.08$ cm^3 dimensions are used for gravimetric measurements. Before all measurements, the exposed area were successively mechanically abraded with 320, 800, 1200 grades of emery papers, washed thoroughly with bidistilled water, cleaned with acetone and dried. Weight loss measurements are carried out in a double walled glass cell equipped with a thermostated cooling

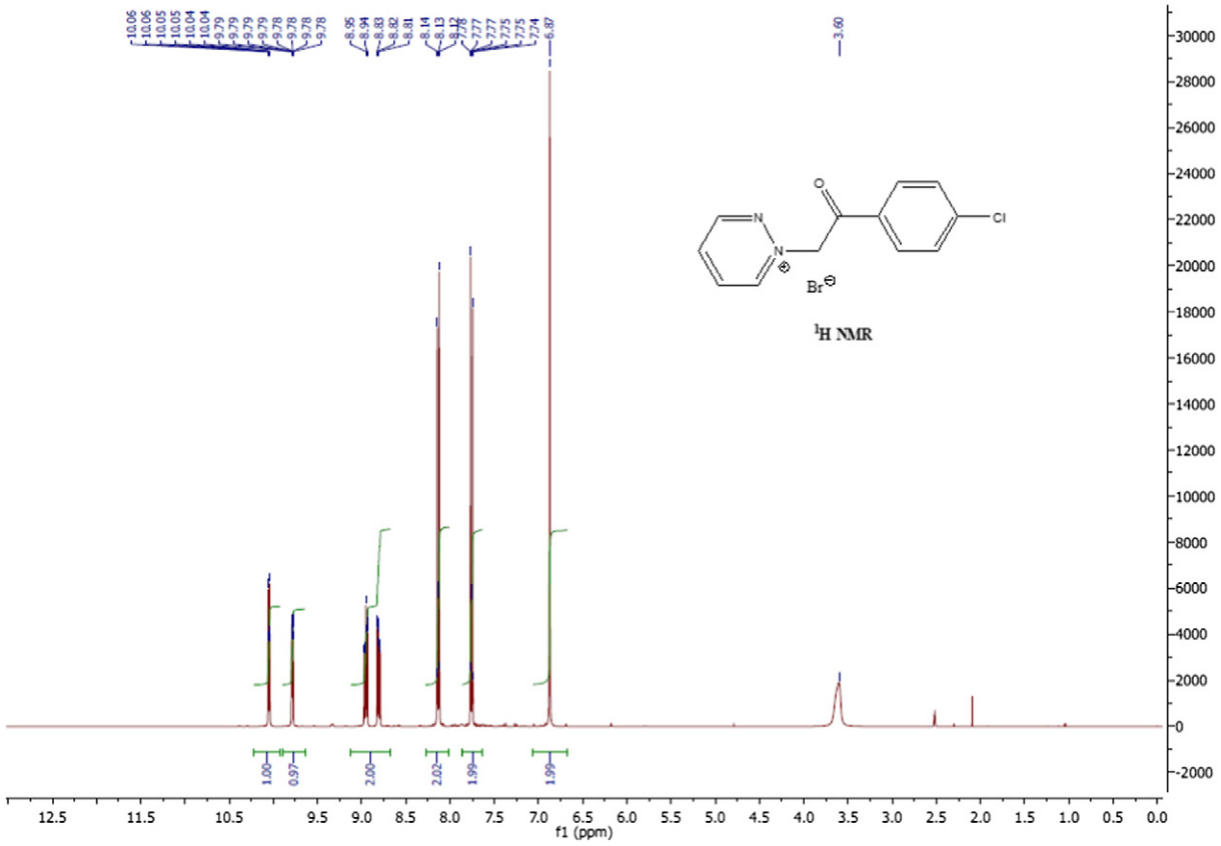

Fig. 2. ^{1}H NMR spectrum of 1-(2-(4-chlorophenyl)-2-oxoethyl)pyridazinium bromide (CPEPB).

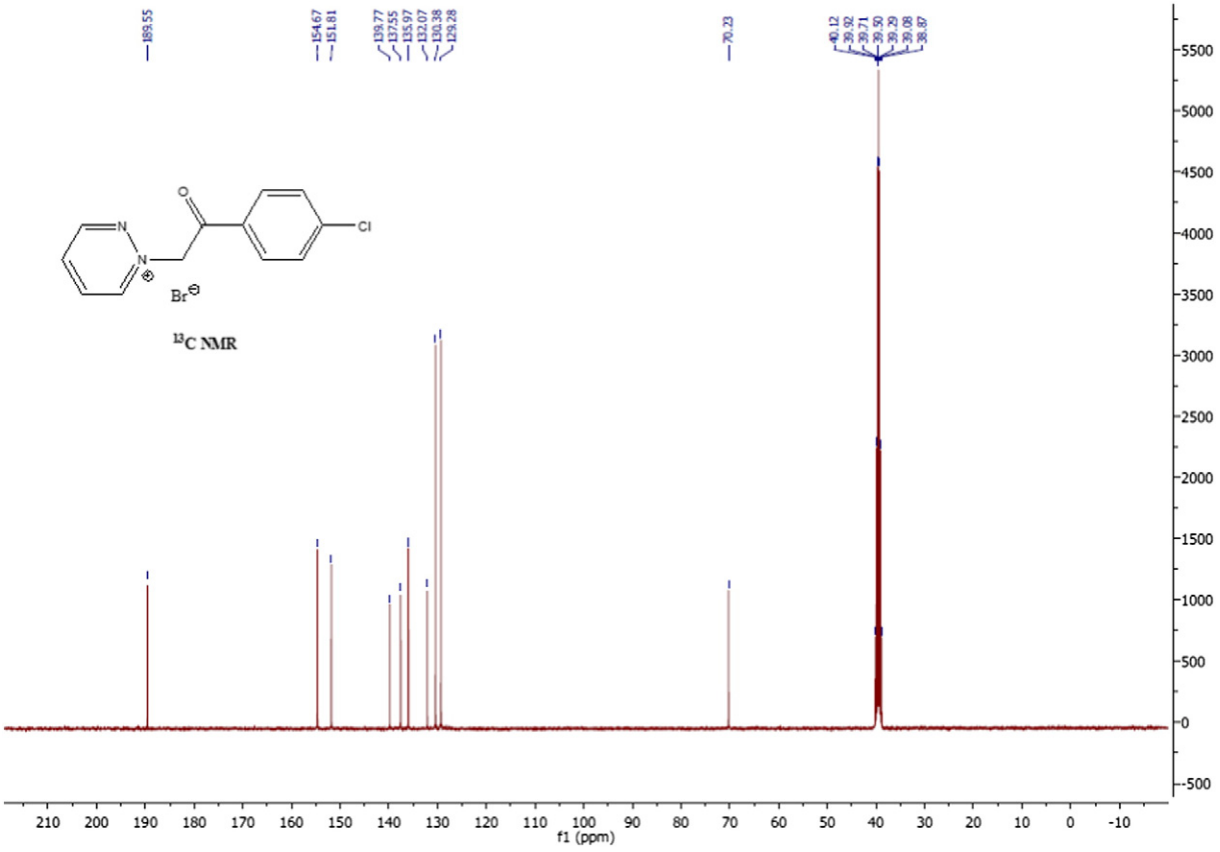

Fig. 3. ^{13}C NMR spectrum of 1-(2-(4-chlorophenyl)-2-oxoethyl)pyridazinium bromide (CPEPB).

condenser. We used 80 mL as the solution volume and fixed the immersion time at 6 h at 298 K for the weight loss.

2.5. Electrochemical measurements

2.5.1. Electrochemical impedance spectroscopy (EIS)

Impedance spectroscopy measurements were carried out using Voltalab (Tacussel-Radiometer PGZ 100) potentiostat and controlled by Tacussel corrosion analysis software model (Voltamaster 4) under static condition. The corrosion cell used had three electrodes. The reference electrode was a saturated calomel electrode (SCE). A platinum electrode was used as auxiliary electrode. The working electrode was carbon steel. All potentials given in this study were referred to this reference electrode. The working electrode was immersed in test solution for 30 min to establish a steady state open circuit potential (Eocp). After measuring the Eocp, the electrochemical measurements were performed. All electrochemical tests have been performed in aerated solutions at 298 K. The response of the electrochemical system to ac excitation with a frequency ranging from 105 Hz to 10–1 Hz and peak to peak amplitude of 10 mV was measured with data density of

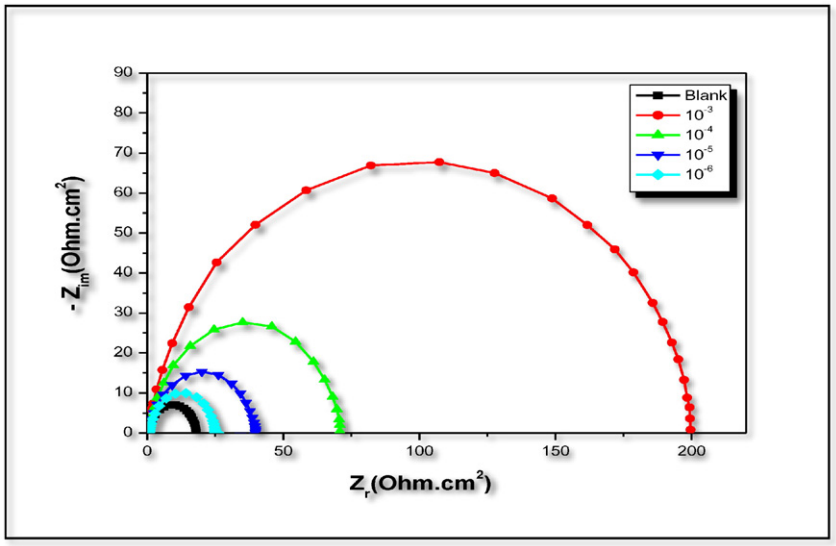

Fig. 4. Nyquist plots for carbon steel in 1 M HCl containing different concentrations of CPEPB.

Table 1
Electrochemical Impedance parameters for corrosion of carbon steel in acid medium at various concentrations of CPEPB.

Inhibitor	Conc. (M)	Rct ($\Omega \cdot cm^2$)	C_{dl} ($\mu F/cm^2$)	E_{Rct} (%)
Blank	1.0	18	176.93	–
CPEPB	1×10^{-3}	200	19.90	91.00
	1×10^{-4}	71	56.07	74.65
	1×10^{-5}	40	62.89	55.00
	1×10^{-6}	25	63.69	28.00

Table 2
Electrochemical parameters of carbon steel in 1.0 M HCl solution with and without CPEPB at different concentrations.

Inhibitor	Conc. (M)	$-E_{corr}$ (mV/SCE)	I_{corr} ($\mu A/cm^2$)	$-b_c$ (mV/dec)	E_I (%)
Blank	1.0	469	588	168	–
CPEPB	1×10^{-3}	516	49	162	91.67
	1×10^{-4}	508	65	154	88.95
	1×10^{-5}	502	90	161	84.69
	1×10^{-6}	489	158	165	73.13

10 points per decade. Nyquist plots were made from these experiments. The best semicircle can be fit through the data points in the Nyquist plot using a non-linear least square fit so as to give the intersections with the x-axis.

2.5.2. Potentiodynamic polarization

The electrochemical behavior of carbon steel sample in inhibited and uninhibited solution was studied by recording anodic and cathodic potentiodynamic polarization curves. Measurements were performed in the 1 M HCl solution containing different concentrations of the tested inhibitor, after 30 min of immersion, by changing the electrode potential automatically from −800 mV to −200 mV versus corrosion potential at a scan rate of 1 $mV \cdot s^{-1}$. The linear Tafel segments of anodic and cathodic curves were extrapolated to corrosion potential to obtain corrosion current densities (I_{corr}).

2.6. Quantum chemical calculations

The quantum theoretical calculations were performed with the Gaussian03 program package [43]. The complete geometry optimization with no constraints of CPEPB of the under taken CPEPB as corrosion inhibitor was performed at DFT (density functional theory) using the hybrid functional B3LYP level taking into account the exchange and the correlation with Beck's three parameters exchange functional along with Lee–Yang–Parr non-local correlation functional [40–42]. All calculations of DFT/B3LYP theory were done using 6-31 g (d,p) orbital basis sets.

2.7. Optical microscopy

Immersion corrosion analysis of carbon steel samples in the acidic media without and with the optimal concentration of the inhibitor was realized by using optical microscopy (OM). Immediately after the corrosion tests, the specimens were subjected to OM studies to examine the surface morphology. The working sample was analyzed at three different locations to ensure reproducibility.

3. Results and discussion

3.1. Electrochemical Impedance Spectroscopy

The corrosion behavior of carbon steel in 1.0 M HCl solution in the presence of CPEPB was investigated by EIS at room temperature after 30 min of immersion. Nyquist diagram obtained at the interface of electrode in the absence and presence of CPEPB at different concentrations for carbon steel are given in Fig. 4.

This figure show the Nyquist diagram contain a single depressed semicircle with the center below the real x-axis, which is size increased by increasing the inhibitor concentrations, this results show that the corrosion process is mainly a charge transfer controlled and the inhibitive film formed was enhanced by the addition of the inhibitor concentrations [44]. The depressed semicircle is the characteristic of electrode surface and often attributed to the frequency dispersion as a result of impurities, roughness and inhomogenates of the electrode surface [45]. Often, it should be noted that the change of concentration of CPEPB does not modify the style of the curves of impedance, which suggests a similar mechanism of inhibitions implied. The data obtained of the Nyquist plots are given in Table 1.

Again, at the concentration of 10^{-3} M, the maximum percentage of inhibition efficiency (E_{Rct} %) was achieved (91%).

According to the Eq. (1), this inhibition efficiency is calculated by charge transfer resistance obtained from Nyquist diagram:

$$E_{Rct}\ \% = \frac{R'_{ct} - R_{ct}}{R'_{ct}} \times 100. \quad (1)$$

Where R_t and R'_t are the charge transfer resistance values without and with inhibitor, respectively.

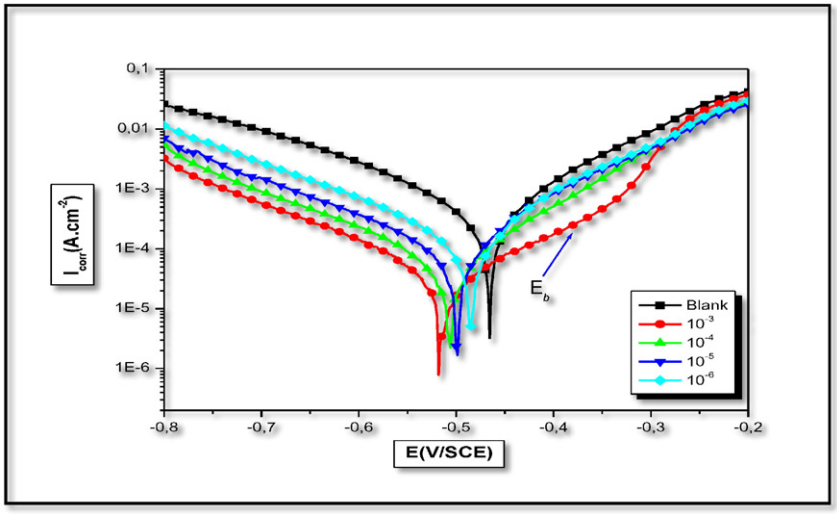

Fig. 5. Potentiodynamic polarization curves of carbon steel in 1 M HCl in the presence of different concentrations of CPEPB at 298 K.

Table 3
Weight loss data of carbon steel in 1.0 M HCl for various concentration of the CPEPB.

Inhibitor	Conc. (M)	W_{corr} (mg·cm^{-2} h^{-1})	E_w (%)	θ
Blank	0	1.001	–	–
CPEPB	1×10^{-3}	0.095	90.51	0.905
	1×10^{-4}	0.110	89.01	0.890
	1×10^{-5}	0.120	88.01	0.880
	1×10^{-6}	0.150	85.01	0.850

3.2. Potentiodynamic polarization curves

Potentiodynamic anodic and cathodic polarization scans were carried out at 289 K in 1.0 M HCl with different concentrations of CPEPB shown in Fig. 5. Table 2 gives the values of electrochemical parameters as the corrosion potential E_{corr}, corrosion current density I_{corr}, Tafel slope b_c, and inhibition efficiency for the corrosion of carbon steel in 1 M HCl with different concentrations of CPEPB. The corrosion current densities were estimated by Tafel extrapolation of the cathodic curves to the open circuit corrosion potential. The inhibition efficiency was then calculated using the expression 2:

$$E_I\% = \frac{I^0_{corr} - I_{corr}}{I^0_{corr}} \times 100 \quad (2)$$

where I^0_{corr} is the corrosion current density in uninhibited acid and I_{corr} is the corrosion current density in inhibited acid.

Data as reported in Table 2 show that the corrosion process was inhibited by the presence of CPEPB inhibitor in the studied range of concentrations and E (%) increases with concentration of the inhibitor, reaching its maximum value, 91.67%, at 10^{-3} M. The values of the cathodic Tafel lines b_c, show slight changes with the addition of CPEPB. The results given in Fig. 5 and from Table 2 indicate that the corrosion potential is more negative and the corrosion current density (I_{corr}) decreases in the presence of an inhibitor compared to the blank solution and also with the increasing inhibitor concentration which suggest that the presence of this compound retards the dissolution of carbon steel electrodes in a 1 M HCl solution. Both anodic and cathodic polarizations are influenced simultaneously, almost to the same extent, which indicate the influence of CPEPB on both the anodic and the cathodic reactions; hydrogen evolution and metal dissolution. This implies that CPEPB affected both the anodic dissolution of carbon steel electrodes and it's cathodic reduction in hydrogen evolution reactions, indicating that the CPEPB compound could be classified as a mixed-type inhibitor. Moreover, the recorded polarization curves in the presence of inhibitor are characterized by the presence of anodic breakdown potential E_b. The noble shift of E_b and the decrease of the corresponding current densities with the increasing inhibitor concentration reflect the formation of anodic protective film on the electrode surface [46]. In addition, the Tafel curves as parallel cathodic in Fig. 5 show that the reduction mechanism is not affected by the presence of the inhibitor and the hydrogen evolution is activation controlled [47].

Table 4
The thermodynamic parameters for the corrosion of carbon steel in 1.0 M HCl in the absence and presence of different concentrations of CPEPB.

Inhibitor	Slope	K_{ads} (M^{-1})	R^2	ΔG_{ads} (kJ/mol)
CPEPB	1.095	9.64×10^5	0.9999	−44.07

3.3. Gravimetric measurements and adsorption isotherm

According to the method described previously, weight loss measurement was carried out [48]. The entire specimen was conducted in aerated 1.0 M HCl solution at 298 K with different concentrations of CPEPB. At the end of the tests the samples were carefully washed in acetone and then weighed. Duplicate experiments were performed in each and the mean value of the weight loss has been reported. After 6 h of immersion, the values of the corrosion rate and the inhibition efficiency obtained from the weight loss measurements of carbon steel for different concentrations of CPEPB in 1.0 M HCl at 298 K are given in Table 3. The inhibition efficiency (Ew %) and surface coverage (θ) were determined by using the following equations:

$$E_w\% = \frac{W_{corr} - W'_{corr}}{W_{corr}} \times 100. \quad (3)$$

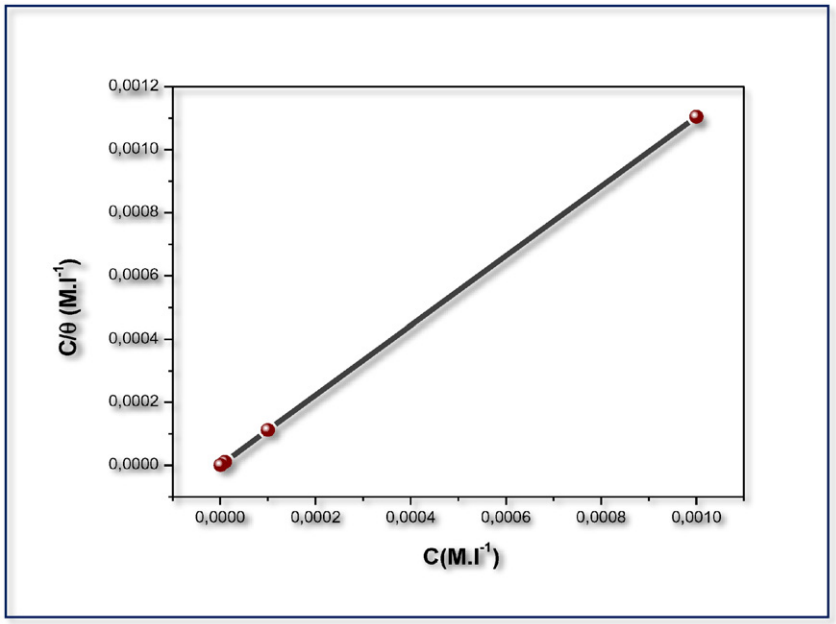

Fig. 6. Langmuir adsorption isotherm of CPEPB inhibitor on the carbon steel surface at 298 K.

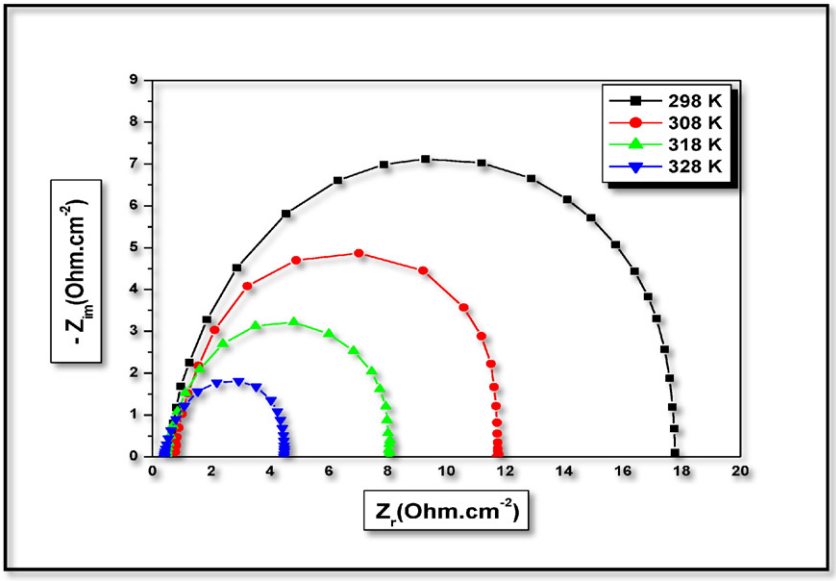

Fig. 7. Nyquist diagrams for carbon steel in 1.0 M HCl at different temperatures.

$$\theta = 1\text{-}\frac{W'corr}{Wcorr} \tag{4}$$

where W'_{corr} and W_{corr} are the corrosion rates of carbon steel in the presence and the absence of definite concentration of inhibitor, respectively, and θ is the degree of surface coverage of the inhibitor.

Results given in Table 3 show that inhibitor CPEPB inhibits the corrosion rat of carbon steel electrode and the efficiency increases with the increasing inhibitor concentration. The efficiency of carbon steel increases with the increase of CPEPB concentration up to 91.21% at 298 K. These corrosion weight loss tests were in good agreement with impedance measurements and the polarization curves method. Basic information about the properties of the tested compound may be provided from the kind of adsorption isotherm. The values of surface coverage θ, corresponding to different concentrations of inhibitors at 298 K have been used to explain the best isotherm to determine the adsorption isotherm of the inhibitor on the surface of electrode. Langmuir adsorption isotherm was found to provide the best description of the adsorption behavior of the investigated inhibitor. The Langmuir isotherm is given by Eq. (5) [49].

$$\frac{C}{\theta} = \frac{1}{K} + C. \tag{5}$$

Where C is the corrosion inhibitor concentration in the solution and K is the adsorption/desorption equilibrium constant.

$$\log K = -1,74 - \left(-\frac{\Delta G_{ads}}{2,303RT}\right). \tag{6}$$

Where ΔG_{ads} present the free energy of adsorption.

It was clear that Fig. 6 (plot of $\frac{\theta}{C}$ versus C) gives straight line with slope near to 1, indicating that the adsorption of compound on carbon steel/acidic solution interface obeys Langmuir's adsorption.

Thermodynamic parameters for adsorption processes obtained from Langmuir's adsorption isotherm for the studied inhibitor are given in

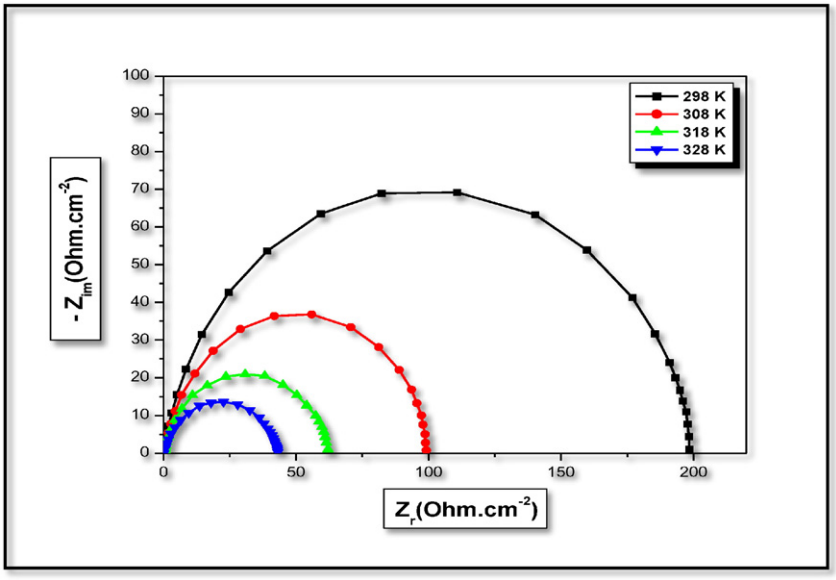

Fig. 8. Nyquist diagrams for carbon steel in 1 M HCl + 10^{-3} M of CPEPB at different temperatures.

Table 5
Thermodynamic parameters for the adsorption of (CPEPB) in 1.0 M HCl on the C38 steel at different temperatures.

Inhibitor	Temp (K)	R_{ct} ($\Omega \cdot cm^2$)	C_{dl} ($\mu F/cm^2$)	E_{Rct} (%)
Blank	298	18	177	–
	308	12	190	–
	318	8	199	–
	328	4.5	223	–
CPEPB	298	200	199	91.00
	308	99	253	87.88
	318	63.5	251	87.40
	328	35.5	449	87.32

Table 4. The free value of the energy of adsorption as calculated from Eq. (6), the free value of $\Delta G_{ads} = -44.07$ kJ mol^{-1} is found to be too negative indicating that CPEPB is strongly adsorbed on the electrode surface and guaranteeing the spontaneity of the adsorption process and stability of the adsorbed layer on the steel surface [50]. The value of ΔG_{ads} is found to be around -40 kJ mol^{-1}; meaning that the adsorption mechanism of CPEPB on carbon steel surface is mainly the chemisorption. Noticeably, it is generally accepted that physical adsorption is a preceding stage of chemisorption of inhibitor on metal surface [51], i.e., chemisorption is always accompanied by physisorption [52].

3.4. Effect of temperature

The study on the effect of temperature on the corrosion rate and inhibition efficiency facilitates the calculation of kinetic and thermodynamic parameters for the inhibition and the adsorption processes. These parameters are useful in interpreting the type of adsorption by the inhibitor. To calculate the activation energies and to investigate the mechanism of inhibition of the corrosion process, electrochemical impedance spectroscopy measurement was taken at various temperatures in the presence and absence the of 10^{-3} M of CPEPB (Figs. 7 and 8).

The results reported in Table 5 showed that the R_{ct} (resistance transfer) values decreases with the increasing temperature in the absence and the presence of CPEPB. Values of R_{ct} were used to calculate the corrosion current density (I_{corr}) values at various temperatures in the presence and absence of CPEPB by using Eq. (7) [53]:

$$I_{corr} = R.T(z.F.R_{ct})^{-1}. \quad (7)$$

Where R_{ct} is the charge transfer resistance, z is the valence of iron ($z = 2$), T is the absolute temperature, F is the Faraday constant ($F = 96.485$ °C) and R is the universal gas constant ($R = 8.31$ J K^{-1} mol^{-1}).

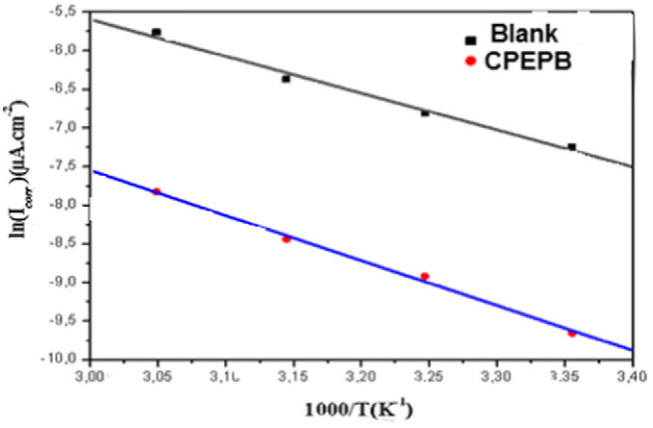

Fig. 9. Arrhenius plots of C38 steel in 1 M HCl with and without 10^{-3} M of CPEPB.

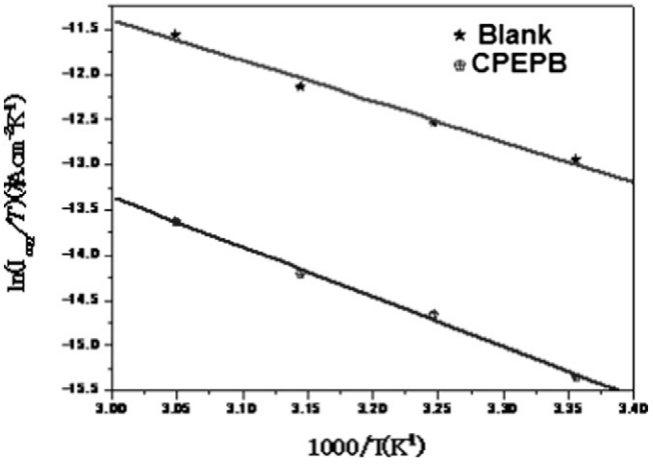

Fig. 10. Relation between Ln (I_{corr}/T) and 1000/T at different temperatures.

The activation parameters for the corrosion process were calculated from Arrhenius type plot according to the following equations (Eqs. (8), (9)):

$$I_{corr} = A \exp\left(-\frac{E_a}{RT}\right). \quad (8)$$

$$I_{corr} = \frac{RT}{Nh} \exp\left(\frac{\Delta S_a^*}{R}\right) \exp\left(\frac{\Delta H_a^*}{RT}\right) \quad (9)$$

where E_a is the apparent activation corrosion energy, A is Arrhenius factor, h is the Plank's constant, N is the Avogadro's number, and ΔH_a^* and ΔS_a^* are the enthalpy and the entropy changes of activation corrosion energies for the transition.

R is the perfect gas constant. The apparent activation energy was determined from the slopes of Ln I_{corr} vs 1/T graph given in Fig. 9.

A plot of ln (I_{corr}/T) against 1/T (Fig. 10) gave a straight line with slope (ΔH_a^*/R) and intercept (ln(R/N A h) + (ΔS_a^*/R)), from which the values of ΔH_a^* and ΔS_a^* were calculated and listed in Table 6.

The increase in activation energy (E_a) of inhibited solutions compared to the blank suggests that inhibitor is physically adsorbed on the corroding electrode surface, whereas either unchanged or lower energy of activation in the presence of inhibitor suggest chemisorption [54]. As reported in Table 6, E_a values increased greatly after the addition of the inhibitor. Hence corrosion inhibition of CPEPB is primarily occurring through physical adsorption. The positive signs of ΔH_a^* reflected the endothermic nature of the electrode dissolution process. The value of ΔS_a^* is lower for the uninhibited solution than that for the inhibited solution. This phenomenon suggested that a decrease in randomness occurred on going from reactants to the activated complex. This could be the result of the adsorption of organic inhibitor molecule from the acidic solution which could be regarded as a quasi-substitution process between the organic compound in the aqueous phase and water molecules at electrode surface [55]. The great negative values of entropies

Table 6
Activation parameters for the corrosion of carbon steel in 1.0 M HCl acid with the presence of different concentrations of CPEPB.

Inhibitor	E_a (kJ/mol)	ΔH_a^* (kJ/mol)	ΔS_a^* (J/mol)	$E_a - \Delta H_a^*$ (kJ/mol)
Blank	39.56	36.96	−181.35	2.60
CPEPB	48.37	45.77	−171.16	2.60

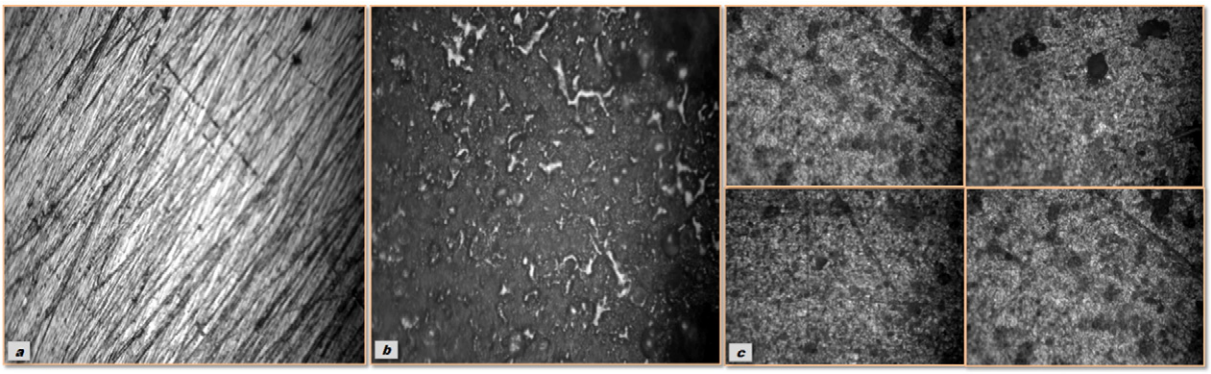

Fig. 11. OM (×200) of tinplate (a) before immersion, (b) after 6 h of immersion in 1 M HCl and (c) after 6 h of immersion in 1 M HCl + 10^{-3} M of CPEPB.

indicate that the activated complex in the rate determining step is an association rather than dissociation step meaning that a decrease in disordering takes place on going from reactants to the activated complex [56,57].

3.5. Optical microscopy

Fig. 11 presents a optical microscopy (OM) image obtained on the carbon steel surface before immersion and after its immersion in 1.0 M HCl without and with the addition of the inhibitor CPEPB at 10^{-3} M during 6 h at 298 K. From Fig. 11a, it can be seen that the fresh carbon steel surface state was uniform. Nevertheless, after immersion a radical change of the surface state is observed. In the case the absence of inhibitor the surface state was strongly damaged due to some cracks and pits as a result of the attack of corrosive solution (Fig. 11b). In the presence of CPEPB inhibitor, OM micrograph showed in Fig. 11c provides the formation of thick films on carbon steel surface. It is revealed that there is a good protective layer adsorbed on the specimen's surface which is responsible for the inhibition of corrosion.

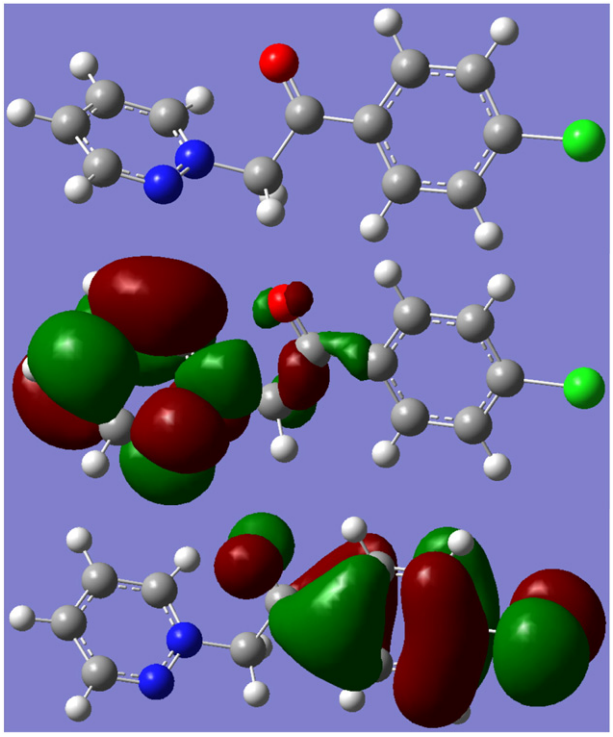

Fig. 12. Optimized structure, LUMO and HOMO of CPEPB.

3.6. Quantum chemical calculations

The optimized geometry at the B3lyp/6–31 g (d, p) level of CPEPB and their corresponding frontier molecular orbitals (LUMO and HOMO) are shown in Fig. 12. The energy levels viz., E_{HOMO}, E_{LUMO} and ΔE calculated in atomic units (u.a. or Hartree) are presented in Table 7.

The LUMO and the HOMO are important to investigate because they provide an idea about the regions of the molecule with the tendency to donate or accept electrons. From Fig. 12, the HOMO is localized on the benzene ring as well as on the carbonyl group and the chlorine atom. The presence of the methylene group breaks the planarity of the molecule CPEPB and thus prevents the HOMO to be delocalized on the entire molecule. Conversely, the orbital LUMO densities are mainly localized on the pyridazinium ring. The calculated Mulliken charges on the atoms give more information on the reactivity sites. The highest negative charge is found on the oxygen atom (−0.453) indicating that this is the atom on which the electrophilic attack would preferably occur. Remarkably, the charge gradient is maximum for the oxygen atom with the carbon atom (0.387) in the carbonyl group.

An ideal corrosion inhibitor has a greater tendency to receive electrons, donate electrons or bind strongly to the metal surface [58] which suggests that CPEPB may donate electrons to the electrode surface through HOMO (chloro phenyl and carbonyl moieties) and accept electrons from the electrode surface through LUMO (pyridazinium ring). Also, the value of E_{HOMO} for CPEPB inhibitor was found to be −0.36301 a.u, which was higher (less negative) compared to that of the iron value (−0.20181). The literature shows that E_{HOMO} is frequently associated with the electron donor ability of the molecule and the inhibition efficiency increases with increase in the values of E_{HOMO}. A higher value of E_{HOMO} for CPEPB than of iron suggests that it has a greater potential to give electrons [59]. From Table 7, it is clear that the energy gap values follow the order, Fe < CPEPB < Fe^{2+} < Fe^{3+}; which suggested that CPEPB has an ability to donate electrons preferably to Fe^{3+} and Fe^{2+}. So, the molecular modeling shows the corrosion inhibition potential of CPEPB while its possible mode of interaction with metal surface.

Table 7
Calculated quantum chemical parameters for CPEPB and iron (Fe, Fe^{2+} and Fe^{3+}).

Compound	E_{HOMO} (a.u.)	E_{LUMO} (a.u.)	$\Delta E = E_{LUMO} - E_{HOMO}$ (a.u.)
CPEPB	−0.36301	−0.25536	0.10765
Fe	−0.20181	−0.12376	0.07805
Fe^{2+}	−1.00063	−0.70608	0.29455
Fe^{3+}	−1.76592	−1.12498	0.64094

4. Conclusion

The CPEPB inhibitor studied in this work shows excellent inhibition properties for the corrosion of carbon steel in 1.0 M HCl at 298 K, and the inhibition efficiency decreases with the decreasing of the CPEPB concentration. The inhibition efficiency dependence of the concentration as calculated from electrochemical studies and weight loss measurements were in good agreement. Based on the polarization results, the investigated CPEPB acts predominantly as a mixed-type inhibitor. The adsorption of CPEPB on the steel electrode surface in 1.0 M chlorodric acid obeys the Langmuir adsorption isotherm model and leads to the formation of a solid protective film. The value of apparent activation energy increases with the increase in the inhibitor concentration. Enthalpy of activation reflects the endothermic nature of Carsteel dissolution process. The inhibition efficiency of CPEPB is temperature-dependant, and inhibition efficiency decreases slightly with the increase in the temperature. CPEPB possibly will offer electrons to the electrode surface through HOMO (chloro phenyl and carbonyl moieties) and receive electrons from the electrode surface through LUMO (pyridazinium ring).

Acknowledgment

Prof. Y. KARZAZI extends his appreciation to the Laboratory for Chemistry of Novel Materials, University of Mons, Belgium, for access to the computational facility.

References

[1] I. Ahamad, R. Prasad, M.A. Quraishi, Corros. Sci. 52 (2010) 3033.
[2] M. Bouklah, B. Hammouti, M. Benkaddour, T. Benhadda, J. Appl. Electrochem. 35 (2005) 1095.
[3] A. Fiala, A. Chibani, A. Darchen, A. Boulkamh, K. Djebbar, Appl. Surf. Sci. 253 (2007) 9347.
[4] A.S. Fouda, A.A. Al-Sarawy, E.E. El-Katori, Desalination 201 (2006) 1.
[5] I. Ahamad, R. Prasad, M.A. Quraishi, Corros. Sci. 52 (2010) 1472.
[6] D.K. Yadav, B. Maiti, M.A. Quraishi, Corros. Sci. 52 (2010) 3586.
[7] S. Edrah, S.K. Hasan, J. Appl. Sci. Res. 6 (2010) 1045.
[8] Y.J. Tan, S. Bailey, B. Kinsella, Corros. Sci. 38 (1996) 1681.
[9] M. Dahmani, A. Et-Touhami, S.S. Al-Deyab, B. Hammouti, A. Bouyanzer, Int. J. ELectrochem. Sci. 5 (2010) 1060.
[10] A.Y. Musa, A.A.H. Kadhum, A.B. Mohamad, M.S. Takriff, A.R. Daud, S.K. Kamarudin, Corros. Sci. 52 (2010) 526.
[11] E.M. Sherif, S.M. Park, J. Electrochem. Soc. 152 (2005) B428.
[12] E.M. Sherif, S.M. Park, Electrochim. Acta 51 (2006) 1313.
[13] S.A. Abd El-Maksoud, A.S. Fouda, Mater. Chem. Phys. 93 (2005) 84.
[14] A.P. Srikanth, T.G. Sunitha, V. Raman, S. Nanjundan, N. Rajendran, Mater. Chem. Phys. 103 (2007) 241.
[15] M. Bouklah, A. Attayibat, B. Hammouti, A. Ramdani, S. Radi, M. Benkaddour, Appl. Surf. Sci. 240 (2005) 341.
[16] R.D. Rogers, K.R. Seddon, Science 302 (2003) 792.
[17] N. Jain, A. Kumar, S. Chauhan, S.M.S. Chauhan, Tetrahedron 61 (2005) 1015.
[18] J.S. Wilkes, Green Chem. 4 (2002) 73.
[19] H.L. Ngo, K. Le Compte, L. Hargens, A.B. McEwen, Thermochim. Acta 97 (2000) 357.
[20] P. Bonhôte, A.-P. Dias, N. Papageorgiou, K. Kalyanasundaram, M. Gratzel, Inorg. Chem. 35 (1996) 1168.
[21] K.M. Dieter, C.J. Dyme, N.E. Heimer, J.W. Rovang, J.S. Wilkes, J. Am. Chem. Soc. 110 (1988) 2722.
[22] S.A. Forsyth, J.M. Pringle, D.R. MacFarlane, Aust. J. Chem. 57 (2004) 113.
[23] F. Endres, S.Z. El Abedin, S. Matter, Phys. Chem. Chem. Phys. 8 (2006) 2101.
[24] M.A.M. Ibrahim, M. Messali, 76 (2011) 14.
[25] F.A. Al-Ghamdi, M. Messali, S.A. Ahmed, J. Mater. Environ. Sci. 2 (2011) 215.
[26] R. Hagiwara, Y. Ito, J. Fluor. Chem. 105 (2000) 221.
[27] M. Messali, A. Ahmed Saleh, Green Sustain. Chem. 1 (2011) 70.
[28] N.V. Likhanova, M.A. Domínguez-Aguilar, O. Olivares-Xometl, N. Nav Dorantes, Corros. Sci. 52 (2010) 2088.
[29] M.A. Quraishi, M.Z.A. Rafiquee, S. Khan, N. Saxena, J. Appl. Electroch. (2007) 1162.
[30] M.A.M. Ibrahim, M. Messali, Z. Moussa, A.Y. Alzahrani, S.N. Alamry, Electrochim. Acta 29 (2011) 375.
[31] M. Messali, J. Mater. Environ. Sci. 2 (2011) 174.
[32] M.E. Palomar, C.O. Olivares-Xometl, N.V. Likhanova, J.B. Pérez-Nava, 14 (2011) 211.
[33] S. Ben Aoun, Der Pharma Chem. 5 (2013) 294.
[34] M. Sangeetha, S. Rajendran, J. Sathiyabama, A. Krishnaveni, P. Shanthy, N. Manimaran, B. Shyamaladevi, Port. Electrochim. Acta 29 (6) (2011) 429.
[35] R. Rosliza, H.B. Senin, W.B. Wan Nik, Colloids Surf. 312 (2008) 185.
[36] G.M. Pinto, J. Nayak, A. Nityananda Shetty, Mater. Chem. Phys. 125 (2011) 628.
[37] M. Messali, A. Bousskri, A. Anejjar, R. Salghi, B. Hammouti, Int. J. Electrochem. Sci. 10 (2015) 4551.
[38] L. Messaadia, O. ID El mouden, A. Anejjar, M. Messali, R. Salghi, O. Benali, B. Hammouti, O. Cherkaoui, A. Lallam, J. Mater. Environ. Sci 6 (2015) 606.
[39] R.M. Butnariu, I.I. Mangalagiu, Bioorg. Med. Chem. 17 (2009) 2823.
[40] A.D.J. Becke, Chem. Phys. 96 (1992) 2155.
[41] A.D.J. Becke, Chem. Phys. 98 (1993) 1372.
[42] C. Lee, W. Yang, R.G. Parr, Phys. Rev. B 37 (1988) 785.
[43] M.J. Frisch, G.W. Trucks, H.B. Schlegel, G.E. Scuseria, M.A. Robb, J.R. Cheeseman, G. Scalmani, V. Barone, B. Mennucci, G.A. Petersson, H. Nakatsuji, M. Caricato, X. Li, H.P. Hratchian, A.F. Izmaylov, J. Bloino, G. Zheng, J.L. Sonnenberg, M. Hada, M. Ehara, K. Toyota, R. Fukuda, J. Hasegawa, M. Ishida, T. Nakajima, Y. Honda, O. Kitao, H. Nakai, T. Vreven, J.A. Montgomery, Jr., J.E. Peralta, F. Ogliaro, M. Bearpark, J.J. Heyd, E. Brothers, K.N. Kudin, V.N. Staroverov, T. Keith, R. Kobayashi, J. Normand, K. Raghavachari, A. Rendell, J.C. Burant, S.S. Iyengar, J. Tomasi, M. Cossi, N. Rega, J.M. Millam, M. Klene, J.E. Knox, J.B. Cross, V. Bakken, C. Adamo, J. Jaramillo, R. Gomperts, R.E. Stratmann, O. Yazyev, A.J. Austin, R. Cammi, C. Pomelli, J.W. Ochterski, R.L. Martin, K. Morokuma, V.G. Zakrzewski, G.A. Voth, P. Salvador, J.J. Dannenberg, S. Dapprich, A.D. Daniels, O. Farkas, J.B. Foresman, J.V. Ortiz, J. Cioslowski, D.J. Fox, Gaussian, Inc, Wallingford CT, 2010.
[44] J. Aljourani, K. Raeissi, M.A. Golozar, Corros. Sci. 51 (2009) 1836.
[45] F. Bentiss, M. Lebrini, M. Lagrenee, Corros. Sci. 47 (2005) 2915.
[46] H.H. Hassan, E. Abdelghani, M.A. Amin, Electrochim. Acta 52 (2007) 6359.
[47] F. Bentiss, M. Bouanis, B. Mernari, M. Traisnel, H. Vezin, M. Lagrenee, Appl. Surf. Sci. 253 (2007) 3696.
[48] M. Ajmal, A.S. Mideen, M.A. Quraishi, Corros. Sci. 36 (1994) 79.
[49] B.S. Sanat kumar, J. Nayak, A.N. Shetty, J. Coat. Technol. Res. 4 (2011) 1.
[50] M.H. Hussin, M.J. Kassim, Mater. Chem. Phys. 125 (2011) 461.
[51] F.P. Wang,W.L. Kang, H.M. Jin, Chemical Industrial Engineering Press, Beijing. 52 (2008) 242.
[52] S.T. Zhang, Z.H. Tao, S.G. Liao, F.J. Wu, Corros. Sci. 52 (2010) 3126.
[53] F. Beck, U.A. Kruger, Electrochim. Acta. 41 (1996) 1083.
[54] T. Tsuru, S. Haruyama, B.J. Gijutsu, J. Jpn. Soc. Corros. Eng. 27 (1978) 573.
[55] L. Afia, R. Salghi, A. Zarrouk, H. Zarrok, O. Benali, B. Hammouti, S.S. Al-Deyab, A. Chakir, L. Bazzi, Port. Electrochim. Acta 30 (4) (2012) 267–279.
[56] E.E. Oguzie, Corros. Sci. 49 (2007) 1527 (35).
[57] S. Martinez, I. Stern, Appl. Surf. Sci. 199 (2002) 83.
[58] E.E. Ebenso, M.M. Kabanda, T. Arslan, M. Saracoglu, F. Kandemirli, L.C. Murulana, A.K. Singh, S.K. Shukla, B. Hammouti, K.F. Khaled, M.A. Quraishi, I.B. Obot, N.O. Eddy, Int. J. Electrochem. Sci. 7 (2012) 5643–5676.
[59] H. Hoptop, W.C. Lineberger, Phys. Chem. Ref. Data 14 (1985) 731–750.